

A Two-Photon Ratiometric Fluorescent Probe for Imaging of Hydrogen Peroxide Levels in Rat Organ Tissues

Chang Su Lim⁺, Myoung Ki Cho⁺, Mi Yeon Park, and Hwan Myung Kim^{*[a]}

Hydrogen peroxide (H₂O₂) is important in the regulation of a variety of biological processes and is involved in various diseases. Quantitative measurement of H₂O₂ levels at the subcellular level is important for understanding its positive and negative effects on biological processes. Herein, a two-photon ratiometric fluorescent probe (SHP-Cyto) with a boronate-based carbamate leaving group as the H₂O₂ reactive trigger and 6-(benzo[d]thiazol-2'-yl)-2-(*N,N*-dimethylamino) naphthalene (BTDAN) as the fluorophore was synthesized and examined for its ability to detect cytosolic H₂O₂ in situ. This probe, based on the specific reaction between boronate and H₂O₂, displayed a fluorescent color change (455 to 528 nm) in response to H₂O₂ in the presence of diverse reactive oxygen species in a physiological medium. In addition, ratiometric two-photon microscopy (TPM) images with SHP-Cyto revealed that H₂O₂ levels gradually increased from brain to kidney, skin, heart, lung, and then liver tissues. SHP-Cyto was successfully applied to the imaging of endogenously produced cytosolic H₂O₂ levels in live cells and various rat organs by using TPM.

Hydrogen peroxide (H₂O₂) is well known for its cytotoxicity, inducing cellular damage via oxidative stress.^[1] This damage is linked to the initiation and progression of a number of diseases, including diabetes, atherosclerosis, neurodegenerative diseases such as Alzheimer's and Parkinson's, and cancer.^[2] However, it has recently been shown to function as a eukaryotic signal transduction regulator in various biological processes.^[3,4] Hence, H₂O₂ can have both positive and negative effects, depending on the level of H₂O₂ as well as the cell or tissue type. Precise measurement of H₂O₂ levels is, therefore, important both for the assessment of signal transduction regulation and as an indicator of disease development. In addition, H₂O₂ is known to be associated with the modulation of organelle function and intracellular calcium ion signaling in rat hippocampus.^[5] Furthermore, acute biogenic amine and stimulants such as amphetamine are known to cause an increase in neu-

rotransmission, leading eventually to intracellular H₂O₂ production, which is highly toxic to various organs such as the liver, heart, and kidney. The ability to detect H₂O₂ levels in rat brain and other organs is, therefore, also of great interest.^[6]

There have been numerous reports of probes for the measurement of reactive oxygen species (ROS) and reactive nitrogen species (RNS) in live cells,^[7–11] including boronate oxidation-based H₂O₂ probes for imaging in live cells.^[12] However, most of the fluorescent small-molecule H₂O₂ probes developed to date have been limited to cells and transparent animals such as zebrafish,^[10c] and approaches to detect H₂O₂ levels with high accuracy in non-transparent animals, such as rat organs, are limited. In addition, most of these probes used one-photon microscopy (OPM), which utilizes short excitation wavelengths for imaging. The utility of OPM is limited in deep tissue imaging because of its low penetration depth ($\approx 80 \mu\text{m}$), and it can only be used for short-time imaging, owing to its high excitation energy. These limitations can be overcome by using two-photon microscopy (TPM), an advanced imaging technique that utilizes a lower energy for excitation with two photons, and provides a number of advantages, such as increased penetration depth ($> 500 \mu\text{m}$), localized excitation, and a long imaging time.^[13] Recently, we reported two-photon (TP) mitochondrial-selective probes that can measure H₂O₂ levels in live cells and tissues by using TPM.^[14] However, it is necessary to develop a new TP probe that can detect H₂O₂ levels and distribution in cytosolic regions by using ratiometric observation methods in order to allow quantitative analysis.

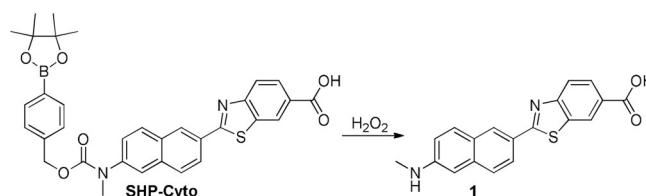
To address this need, we have developed a ratiometric TP probe for cytosolic H₂O₂ (SHP-Cyto, Scheme 1) derived from 6-(benzo[d]thiazol-2'-yl)-2-(*N,N*-dimethylamino) naphthalene (BTDAN) as the fluorophore, with a boronate-based carbamate leaving group as the H₂O₂ reactive trigger. BTDAN shows good TP properties and has been applied in TP probes for metal ions, thiols, and enzymes,^[15,16] and the boronate-based carbamate linkage is widely used as the reaction site for H₂O₂.^[12c] We expected that the cleavage of H₂O₂-triggered boronate and electron-poor carbamate linkage would release the more elec-

[a] Prof. Dr. C. S. Lim,⁺ M. K. Cho,⁺ M. Y. Park, Prof. Dr. H. M. Kim
Department of Energy System Research and Department of Chemistry
Ajou University, Suwon, Gyeonggi-do, 443–749 (Republic of Korea)
E-mail: kimhm@ajou.ac.kr

[⁺] These authors contributed equally to this work

Supporting Information and the ORCID identification number(s) for the author(s) of this article can be found under <https://doi.org/10.1002/open.201700155>.

© 2017 The Authors. Published by Wiley-VCH Verlag GmbH & Co. KGaA. This is an open access article under the terms of the Creative Commons Attribution-NonCommercial License, which permits use, distribution and reproduction in any medium, provided the original work is properly cited and is not used for commercial purposes.



Scheme 1. Structures of SHP-Cyto and 1.

tron-rich structure **1**, which shows red-shifting of the emission spectrum (Scheme 1).

The detailed synthetic procedure of SHP-Cyto is described in the Supporting Information. The solubility of SHP-Cyto, as determined by the fluorescence method,^[17] was 4 μM in MOPS buffer (30 mM MOPS, 100 mM KCl, pH 7.4), which is enough to label cells (Figure S1). Within the soluble range, SHP-Cyto and **1** showed absorption maxima (λ_{abs}) at 333 nm ($\epsilon = 38,000 \text{ M}^{-1} \text{ cm}^{-1}$) and 371 nm ($\epsilon = 21,000 \text{ M}^{-1} \text{ cm}^{-1}$), respectively, and fluorescence maxima (λ_{fl}) at 455 nm ($\Phi = 1.00$) and 528 nm ($\Phi = 0.70$), respectively (Table 1).

Compound	$\lambda_{\text{max}}^{(1)}$ ($10^{-4} \epsilon$) ^[b]	$\lambda_{\text{max}}^{\text{fl}}$ ^[c]	Φ ^[d]	$\lambda_{\text{max}}^{(2)}$ ^[e]	$\Phi\delta$ ^[f]
SHP-Cyto	333 (3.80)	455	1.00	740	14
1	371 (2.10)	528	0.70	750	104

[a] All data were measured in MOPS buffer (30 mM MOPS, 100 mM KCl, pH 7.4) unless otherwise noted. [b] λ_{max} of the one-photon absorption spectra in [nm]. The numbers in parentheses are molar extinction coefficients in [$\text{M}^{-1} \text{ cm}^{-1}$]. [c] λ_{max} of the one-photon emission spectra in [nm]. [d] Fluorescence quantum yield, $\pm 15\%$. [e] The peak two-photon cross section in $10^{-50} \text{ cm}^4 \text{ s photon}^{-1}$ (GM), $\pm 15\%$. [f] Two-photon action cross-section.

Reaction of SHP-Cyto with H_2O_2 produced **1** as the reaction product, as detected by the emission spectra (Figure 1a). Upon addition of 1 mM H_2O_2 to the MOPS buffer, the emission spectra at 455 nm of SHP-Cyto (1 μM) decreased, whereas that at 528 nm increased gradually as a result of the formation of **1**. This process followed pseudo-first-order kinetics with $k_{\text{obs}} = 1.2 \times 10^{-3} \text{ s}^{-1}$ (Figure S2). A similar value was reported in previously developed H_2O_2 probes.^[14] Furthermore, $F_{\text{yellow}}/F_{\text{blue}}$ (530–600 nm/400–470 nm), the ratio of the emission intensities, increased 217-fold (Figure 1a). This result indicates that the emission ratio of SHP-Cyto is highly sensitive to changes in H_2O_2 level, and this sensitivity is higher than those reported in previous studies.^[14] The detection limit of H_2O_2 with SHP-Cyto is 4.0 μM (Figure S3). Moreover, SHP-Cyto has high selectivity for H_2O_2 over competing biological species, ROS, and RNS, as shown by unchanged $F_{\text{yellow}}/F_{\text{blue}}$ ratios following the addition of 200 μM of diverse ROS and RNS, including *tert*-butylhydroperoxide (TBHP), superoxide (O_2^-), hypochlorite (OCl^-), *tert*-butoxy radicals (OtBu), nitric oxide (NO), hydroxyl radicals (OH), and peroxyxynitrite (ONOO^-) (Figure 1b). SHP-Cyto and **1** also exhibit pH insensitivity over the biologically relevant pH range (Figure S4). These results indicate that SHP-Cyto is useful as a ratiometric fluorescent probe for H_2O_2 with minimal interference from other ROS and RNS or from changes in pH.

Next, we estimated the ability of SHP-Cyto to detect H_2O_2 in TP measurements. The TP action ($\Phi\delta$) spectra of SHP-Cyto and **1** in MOPS buffer at pH 7.4 showed $\Phi\delta_{\text{max}}$ values of 14 and 106 GM at 740 and 750 nm, respectively (Figure S5). **1** exhibited a 7.6-fold higher $\Phi\delta_{\text{max}}$ value than SHP-Cyto, in part as a result of enhanced intramolecular charge transfer between the donor and acceptor (vide supra).^[18]

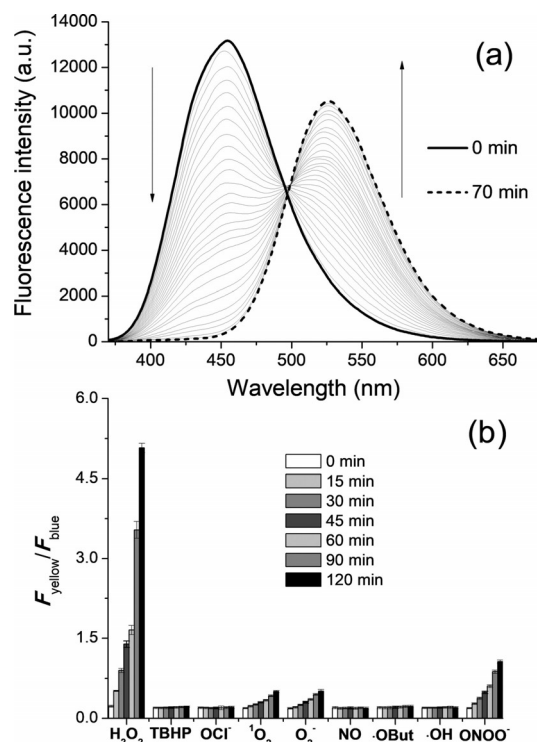


Figure 1. a) One-photon fluorescence response with time for the reactions of SHP-Cyto (1 μM) with H_2O_2 (1 mM). Spectra were acquired at 0 to 70 min after addition of H_2O_2 . b) Fluorescence responses of 1 μM SHP-Cyto to various reactive oxygen and nitrogen species (200 μM). Bars represent the integrated fluorescence ratios $F_{\text{yellow}}/F_{\text{blue}}$ at 0 to 120 min after addition of each reactive species. Data were acquired at 25 $^{\circ}\text{C}$ in 30 mM MOPS, pH 7.4, with excitation wavelength 370 nm.

Subsequently, we applied SHP-Cyto as a TP probe to monitor changes in H_2O_2 levels in cellular environments. For confirmation of its utility in live-cell imaging, SHP-Cyto was used to label HeLa cells. The emission ratio images were generated from two emission channels, 400–470 nm (F_{blue}) and 530–600 nm (F_{yellow}), upon TP excitation at 750 nm, and the emission ratios ($F_{\text{yellow}}/F_{\text{blue}}$) were 0.57 and 2.18 for SHP-Cyto and **1**, respectively (Figures 2a, 2d, and 2e). The $F_{\text{yellow}}/F_{\text{blue}}$ ratio was increased 3.8-fold, and its values were larger than those obtained in previous studies, confirming the high sensitivity of SHP-Cyto as a H_2O_2 probe. In addition, SHP-Cyto showed high sensitivity to changes in H_2O_2 levels: the $F_{\text{yellow}}/F_{\text{blue}}$ ratio increased to 1.49 upon pretreatment with phorbol myristate acetate (PMA), which induces H_2O_2 generation through a cellular inflammation process,^[19] and to 1.85 when the cells were pretreated with 200 μM H_2O_2 for 30 min (Figures 2b, 2c, and 2e). The $F_{\text{yellow}}/F_{\text{blue}}$ ratios were considerably smaller when cells were pretreated with PMA than with excess H_2O_2 . In contrast, the $F_{\text{yellow}}/F_{\text{blue}}$ ratios were very similar for the mitochondrial-selective H_2O_2 probe, that is, SHP-Mito-labeled cells pretreated with excess H_2O_2 and PMA.^[14b] This result distinguishes SHP-Cyto from SHP-Mito in the detection of H_2O_2 in cytosolic environments. In addition, SHP-Cyto was found to be non-toxic to HeLa cells within incubation concentrations, as determined by MTS [3-(4,5-dimethylthiazol-2-yl)-5-(3-carboxymethoxyphenyl)-2-(4-sulfophenyl)-2H-tetrazolium] assay (Figure S6). Furthermore,

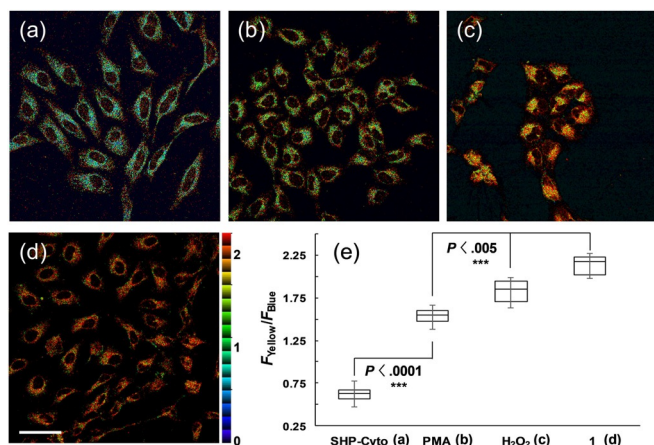


Figure 2. Pseudo-colored ratiometric TPM images ($F_{\text{yellow}}/F_{\text{blue}}$) of HeLa cells incubated with $3 \mu\text{M}$ a) SHP-Cyto and d) 1. Cells were pretreated with b) PMA ($1 \mu\text{g mL}^{-1}$) for 30 min and c) $200 \mu\text{M}$ H₂O₂ for 30 min. e) Box plot of average $F_{\text{yellow}}/F_{\text{blue}}$ in (a)–(d). Images were acquired by using 750 nm excitation and fluorescent emission windows: blue 400–470 nm, yellow 530–600 nm. Scale bar = $60 \mu\text{m}$. Cells shown are representative images from replicate experiments ($n=5$).

SHP-Cyto showed sufficient photostability in HeLa cells for 1 h in two emission detection windows (Figure S7). These results indicate that SHP-Cyto is capable of detecting H₂O₂ levels in live cells.

To further confirm the applicability of SHP-Cyto for bioimaging applications, we applied the probe to the detection of changes in H₂O₂ levels deep inside live tissue. Hippocampus tissue slices were taken from 2-week-old rats, and a slice was labeled with 10 mM SHP-Cyto for 1 h at 37°C . A tile-scanned ratiometric TPM image with $40\times$ magnification was captured and a part of this slice reveals the CA1, CA3, and DG regions (Figures 3b). Hippocampus slice tissues are well known to have an inhomogeneous structure. For that reason, we accumulated 20 TPM images from the two emission channels (F_{blue} , F_{yellow}) at depths of $90\text{--}180 \mu\text{m}$ to visualize the overall H₂O₂ distribution in the tissue. Upon pretreatment of the tissue with 1 mM H₂O₂, the ratio increased gradually from 0.57 to 1.63 (Figures 3a, 3b, and 3d), which lies between the ratios measured in SHP-Cyto- and 1-labeled tissues (Figure 3). Therefore, SHP-Cyto is responsive to changes in H₂O₂ levels in live tissue. Interestingly, the changes in emission ratios measured deep inside the rat brain tissue are comparable to those measured in cultured cells. Moreover, the expanded ratiometric image (white box in whole slice tissue image) clearly reveals the H₂O₂ distribution in the individual cells in the CA3 region at a depth of approximately $120 \mu\text{m}$ (Figures 3a–c). These outcomes demonstrate that SHP-Cyto is capable of detecting changes in H₂O₂ levels in live tissues at depths of $90\text{--}180 \mu\text{m}$ when using TPM.

Finally, we measured the H₂O₂ distribution in several rat organ tissues: brain, kidney, skin, heart, lung, and liver tissues taken from 2-week-old rats. The 20 ratio images of the SHP-Cyto-labeled tissues were accumulated and their emission ratios ($F_{\text{yellow}}/F_{\text{blue}}$) were analyzed (Figure 4a–f). The average levels of $F_{\text{green}}/F_{\text{blue}}$ in response to H₂O₂ in the brain, kidney, skin, heart, lung, and liver tissues were 0.48, 0.76, 0.77, 0.81,

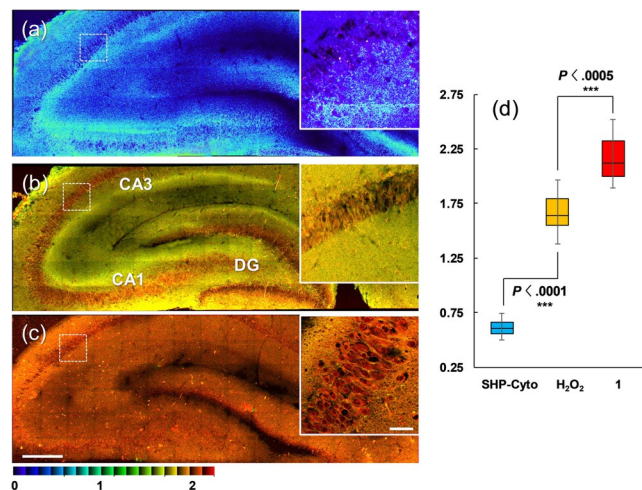


Figure 3. Tile-scanned ratiometric TPM images of a rat hippocampal slice stained with a) $10 \mu\text{M}$ SHP-Cyto and c) 1, and b) pretreated with 1 mM H₂O₂ for 30 min before labeling with $20 \mu\text{M}$ SHP-Cyto. A total of 15 ratiometric TPM images were accumulated along the z direction at depths of approximately $90\text{--}180 \mu\text{m}$ with magnification at $40\times$. The white boxes show enlarged images of the regions in red boxes in (a)–(c) at $120 \mu\text{m}$ depth. d) Box plot of average $F_{\text{yellow}}/F_{\text{blue}}$ in (a)–(c). The TPEF were collected at two channels (blue 400–470 nm, yellow 530–600 nm) upon excitation at 750 nm with a femtosecond pulse. Scale bars: $300 \mu\text{m}$ (a)–(c) and $75 \mu\text{m}$ (inset).

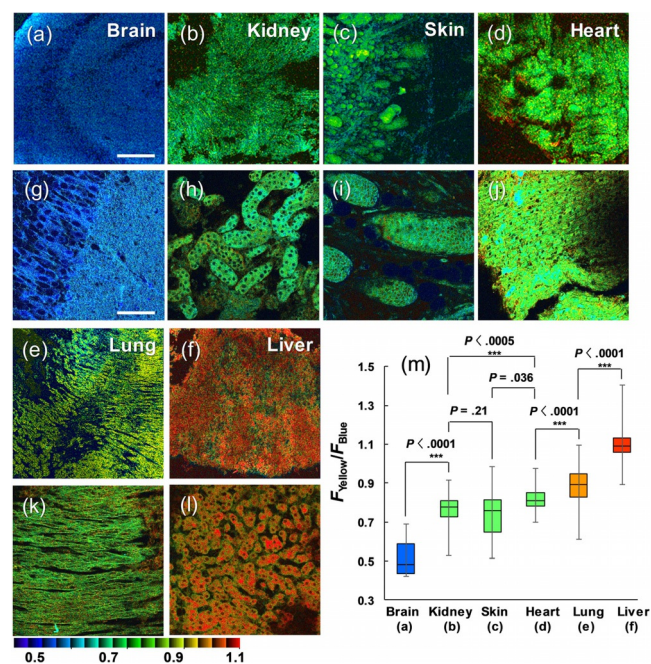


Figure 4. Ratiometric TPM images of the a, g) brain, b, h) kidney, c, i) skin, d, j) heart, e, k) lung, and f, l) liver tissues of rat organs. All tissues were labelled with $20 \mu\text{M}$ SHP-Cyto and a–f) 20 ratiometric TPM images were accumulated along the z direction at the depths of approximately $90\text{--}180 \mu\text{m}$ with magnification at $40\times$. g–l) Enlarged images of (a)–(f) at $120 \mu\text{m}$ depth. m) Box plot of average $F_{\text{yellow}}/F_{\text{blue}}$ in (a)–(l). The TPEF were collected at two channels (blue 400–470 nm, yellow 530–600 nm) upon excitation at 750 nm with a femtosecond pulse. Scale bars: $500 \mu\text{m}$ (a)–(f) and $75 \mu\text{m}$ (g)–(l).

0.89, and 1.09, respectively (Figure 4 m), indicating differences in H₂O₂ level between the organ tissues.^[20,21] This result sug-

gests the utility of SHP-Cyto for the detection of the H₂O₂ level in various live tissues by ratiometric TPM imaging.

To conclude, we have developed a new ratiometric TP probe (SHP-Cyto), which shows a high TP cross-section, a noticeable blue-to-yellow emission color change with high sensitivity to H₂O₂ levels, and high stability over the biologically relevant pH range. This TP probe is able to measure H₂O₂ levels quantitatively in live cells and deep inside various rat organ tissues. The ratiometric TPM images with SHP-Cyto revealed that H₂O₂ levels gradually increase from brain to kidney, skin, heart, lung, and then liver organ tissues. These results indicate that this probe will be useful for applications in studies on the biological role of H₂O₂ and for the diagnosis of various diseases.

Acknowledgements

This work was supported by grants from the National Research Foundation (NRF) funded by the Korean Government (2016R1E1A1A02920873, 2013R1A6A3A04058351, and 20090093826), and the Ajou University research fund.

Conflict of Interest

The authors declare no conflict of interest.

Keywords: hydrogen peroxide · rat organ imaging · ratiometric fluorescent probe · two-photon microscopy · two-photon probe

- [1] a) J. F. Ward, J. W. Evans, C. L. Limoli, P. M. Calabro-Jones, *Br. J. Cancer Suppl.* **1987**, *55*, 105–112; b) J. A. Imlay, *Annu Rev Biochem* **2008**, *77*, 755–776.
- [2] a) T. Finkel, M. Serrano, M. A. Blasco, *Nature* **2007**, *448*, 767–774; b) K. J. Barnham, C. L. Masters, A. I. Bush, *Nat. Rev. Drug. Discov.* **2004**, *3*, 205–214; c) M. T. Lin, M. F. Beal, *Nature* **2006**, *443*, 787–795.
- [3] a) J. F. Turrens, *J. Physiol.* **2003**, *552*, 335–344; b) B. C. Dickinson, C. J. Chang, *Nat. Chem. Biol.* **2011**, *7*, 504–511.
- [4] a) D. Harman, *Proc. Natl. Acad. Sci. USA* **1981**, *78*, 7124–7128; b) T. Finkel, N. J. Holbrook, *Nature* **2000**, *408*, 239–247; c) E. R. Stadtman, *Free Radical Res.* **2006**, *40*, 1250–1258.
- [5] F. J. Gerich, F. Funke, B. Hildebrandt, M. Fasshauer, M. Muller, *Pflugers. Arch.* **2009**, *458*, 937–952.
- [6] F. Carvalho, J. A. Duarte, M. J. Neuparth, H. Carmo, E. Fernandes, F. Remiao, M. L. Bastos, *Arch. Toxicol.* **2001**, *75*, 465–469.
- [7] a) X. Dong, C. H. Heo, S. Chen, H. M. Kim, Z. Liu, *Anal. Chem.* **2013**, *86*, 308–311; b) Z. Mao, H. Jiang, Z. Li, C. Zhong, W. Zhang, Z. Liu, *Chem. Sci.* **2017**, *8*, 4533–4538.
- [8] a) J. Nie, Y. Liu, J. Niu, Z. Ni, W. Lin, *J. Photochem. Photobiol. A* **2017**, *348*, 1–7; b) Y. Liu, J. Niu, J. Nie, F. Meng, W. Lin, *New J. Chem.* **2017**, *41*, 3320–3325; c) M. Ren, B. Deng, K. Zhou, X. Kong, J. Y. Wang, W. Lin, *Anal. Chem.* **2017**, *89*, 552–555.
- [9] a) D. Cheng, Y. Pan, L. Wang, Z. Zeng, L. Yuan, X. Zhang, Y. T. Chang, *J. Am. Chem. Soc.* **2017**, *139*, 285–292; b) L. Yuan, L. Wang, B. K. Agrawala, S. J. Park, H. Zhu, B. Sivaraman, J. Peng, Q. H. Xu, Y. T. Chang, *J. Am. Chem. Soc.* **2015**, *137*, 5930–5938; c) S. W. Lee, H. W. Rhee, Y. T. Chang, J. I. Hong, *Chem. Eur. J.* **2013**, *19*, 14791–14794.
- [10] a) J. Li, C. S. Lim, G. Kim, H. M. Kim, J. Yoon, *Anal. Chem.* **2017**, *89*, 8496–8500; b) A. C. Sedgwick, X. Sun, G. Kim, J. Yoon, S. D. Bull, T. D. James, *Chem. Commun.* **2016**, *52*, 12350–12352; c) Y. Yang, F. Huo, C. Yin, M. Xu, Y. Hu, J. Chao, Y. Zhang, T. E. Glass, J. Yoon, *J. Mater. Chem. B* **2016**, *4*, 5101–5104; d) Q. Xu, C. H. Heo, J. A. Kim, H. S. Lee, Y. Hu, D. Kim, K. M. K. Swamy, G. Kim, S. J. Nam, H. M. Kim, J. Yoon, *Anal. Chem.* **2016**, *88*, 6615–6620.
- [11] a) X. Xie, X. Yang, T. Wu, Y. Li, M. Li, Q. Tan, X. Wang, B. Tang, *Anal. Chem.* **2016**, *88*, 8019–8802; b) R. Bortolozzi, S. V. Gradowski, H. Ihmels, K. Schäfer, G. Viola, *Chem. Commun.* **2014**, *50*, 8242–8245; c) W. Zhang, T. Liu, F. Huo, P. Ning, X. Meng, C. Yin, *Anal. Chem.* **2017**, *89*, 8079–8083.
- [12] a) B. C. Dickinson, C. J. Chang, *J. Am. Chem. Soc.* **2008**, *130*, 9638–9639; b) B. C. Dickinson, Y. Tang, Z. Chang, C. J. Chang, *Chem. Biol.* **2011**, *18*, 943–948; c) A. R. Lippert, G. C. Van De Bittner, C. J. Chang, *Acc. Chem. Res.* **2011**, *44*, 793–804; d) V. Carroll, B. W. Michel, J. Blecha, H. Van-Brocklin, K. Keshari, D. Wilson, C. J. Chang, *J. Am. Chem. Soc.* **2014**, *136*, 14742–14745; e) X. Fu, Y. Tang, B. C. Dickinson, C. J. Chang, Z. Chang, *Biochem. Biophys. Res. Commun.* **2015**, *458*, 896–900; f) L. E. Tomalin, A. M. Day, Z. E. Underwood, G. R. Smith, P. Dalle Pezze, C. Rallis, W. Patel, B. C. Dickinson, J. Bähler, T. F. Brewer, *Free Radical Biol. Med.* **2016**, *95*, 333–348.
- [13] a) W. R. Zipfel, R. M. Williams, W. W. Webb, *Nat. Biotechnol.* **2003**, *21*, 1369–1377; b) F. Helmchen, W. Denk, *Nat. Methods* **2005**, *2*, 932–940; c) H. M. Kim, B. R. Cho, *Chem. Rev.* **2015**, *115*, 5014–5055.
- [14] a) C. Chung, D. Srikun, C. S. Lim, C. J. Chang, B. R. Cho, *Chem. Commun.* **2011**, *47*, 9618–9620; b) G. Masanta, C. H. Heo, C. S. Lim, S. K. Bae, B. R. Cho, H. M. Kim, *Chem. Commun.* **2012**, *48*, 3518–3520.
- [15] a) H. J. Kim, C. S. Lim, H. W. Lee, H. S. Lee, Y. J. Um, H. Kumar, I. Han, H. M. Kim, *Biomaterials* **2017**, *141*, 251–259; b) S. K. Bae, C. H. Heo, D. J. Choi, D. Sen, E. H. Joe, B. R. Cho, H. M. Kim, *J. Am. Chem. Soc.* **2013**, *135*, 9915–9923.
- [16] a) H. W. Lee, C. H. Heo, D. Sen, H. O. Byun, I. H. Kwak, G. Yoon, H. M. Kim, *Anal. Chem.* **2014**, *86*, 10001–10005; b) S. J. Park, H. W. Lee, H. Kim, C. Kang, H. M. Kim, *Chem. Sci.* **2016**, *7*, 3703–3709.
- [17] H. M. Kim, H. J. Choo, S. Y. Jung, Y. G. Ko, W. H. Park, S. J. Jeon, C. H. Kim, T. Joo, B. R. Cho, *ChemBioChem* **2007**, *8*, 553–559.
- [18] H. M. Kim, B. R. Cho, *Chem. Commun.* **2009**, *2*, 153–164.
- [19] M. C. Carreras, G. A. Pargament, S. D. Catz, J. J. Poderoso, A. Boveris, *FEBS Lett.* **1994**, *341*, 65–68.
- [20] a) J. Wilhelm, M. Frydrychova, M. Vizek, *Physiol. Res.* **1999**, *48*, 445–449; b) W. J. Piotrowski, T. Pietras, Z. Kurmanowska, D. Nowak, J. Marczak, J. Marks-Konczalik, P. Mazerant, *J. Appl. Toxicol.* **1996**, *16*, 501–507.
- [21] a) B. Halliwell, M. V. Clement, L. H. Long, *FEBS Lett.* **2000**, *486*, 10–13; b) T. P. Szatrowski, C. F. Nathan, *Cancer Res.* **1991**, *51*, 794–798.

Received: September 22, 2017
Version of record online November 22, 2017